Supporting information

Nano-cobalt anchored on chitosan-derived N-doped porous carbon: an efficient catalyst for α-alkylation of ketones with alcohols *via* borrowing hydrogen

Zegang Zhang[1], Dongbin Mo[1], Youjuan Tan[1], Xueqin Chang[1], Lin Chen[1,*], Xianglin Pei[1,*]

[1.] School of Chemistry and Materials Science, School of Materials and Architectural Engineering, Guizhou Normal University, Guiyang 550025, China.

* Corresponding Author: L. Chen, E-mail: chenlin8310@aliyun.com; X. Pei, E-mail: xianglinpei@163.com.

Table of contents

1. Materials

Chitosan (90% deacetylation rate) was purchased from Ruji Biotechnology. Cobalt chloride hexahydrate ($CoCl_2 \cdot 6H_2O$, 98% purity) was obtained from Bide Pharmaceutical. Other reagents were also procured from commercial suppliers, including Bode, Aladdin, Maclin, Meichi, J&K, Energy, and Chuandong, and were used directly without further purification. The reaction progress was monitored by gas chromatography (GC) using a Shimadzu GC-2014+AFSC equipped with an FID detector (230 °C) or by thin-layer chromatography (TLC) using Huanghai HSGF254 silica gel plates. Column chromatography separation was performed using Haiyang silica gel G (300-400 mesh) as the stationary phase.

2. Characterization

The morphology of the samples was examined using a field emission scanning electron microscope (FESEM, Zeiss SUPRA 55 Sapphire, Germany) at an acceleration voltage of 5 kV. Nitrogen adsorption measurements were performed using a Micromeritics AsAp2020 (USA) with automated Brunauer-Emmett-Teller (BET) and Barrett-Joyner-Halenda (BJH) analyses. The BJH analysis was conducted on the desorption branch of the isotherm. X-ray diffraction (XRD) patterns were recorded on an X-ray powder diffractometer (Rigaku Miniflex600, Japan) with Cu Kα radiation (λ = 1.5406 Å). Infrared spectra were acquired using a Fourier transform infrared spectrometer (FT-IR, PerkinElmer Corporation/model 1600, USA). X-ray photoelectron spectroscopy (XPS) data were collected on a VG Multi Lab 2000 system equipped with a monochromatic Al Kα X-ray source (XPS, VG Multi Lab 2000, USA). Transmission electron microscopy (TEM) images were recorded using a JEM-2010 electron microscope (JEOL, Japan) at an acceleration voltage of 200 kV. Co loading was determined using ICP-OES (Prodigy 7, Leeman Labs Inc., USA). ^{1}H-NMR spectra were recorded at 300 MHz or 400 MHz, respectively, using Bruker AVANCE 300 and 400 spectrometers, with $CDCl_3$ (7.26 ppm) as a solvent. ^{13}C NMR spectra were acquired at 75 or 100 MHz, referenced to the internal solvent signals ($CDCl_3$ with central peaks at 77.16 ppm, respectively). Chemical shifts and coupling constants (*J*) are reported using ppm and Hz, respectively. Peak multiplicity is denoted as follows: s (single peak), d (double peak), t (triple peak), m (multiple peaks).

3. Computational details

We carried out all the DFT calculations in the Vienna *ab initio* simulation (VASP5.4.4) code.[1] The exchange-correlation is simulated with PBE functional and the ion-electron interactions were described by the PAW method.[2,3] The vdWs interaction was included by using empirical DFT-D3 method.[4] The Monkhorst-Pack-grid-mesh-based Brillouin zone k-points are set as 1×1×1 for all periodic structure with the cutoff energy of 400 eV. Partial occupancies of the Kohn−Sham orbitals were allowed using the Gaussian smearing method with a width of 0.05 eV.The convergence criteria are set as 0.05 eV A^{-1} and 10^{-5} eV in force and energy, respectively.

The adsorption energy calculation of species adsorption (E_{ads})

$$E_{ads} = E_{adsorbate/surface} - E_{adsorbate} - E_{surface} \quad (1)$$

Where $E_{adsorbate/surface}$ is the total energy of the surface with the adsorbate adsorbed, $E_{adsorbate}$ is the total energy of the isolated adsorbate, and $E_{surface}$ is the total energy of the bare surface. A negative value for the adsorption energy indicates that the adsorption process is exothermic.

4. Figures

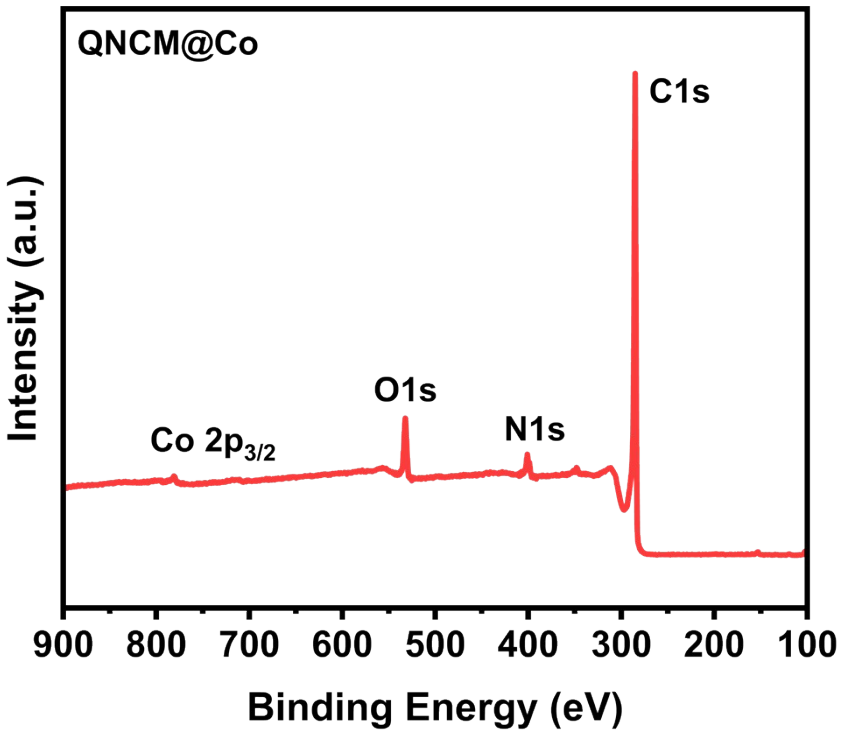

Figure S1. Full-size XPS spectra of QNCM@Co

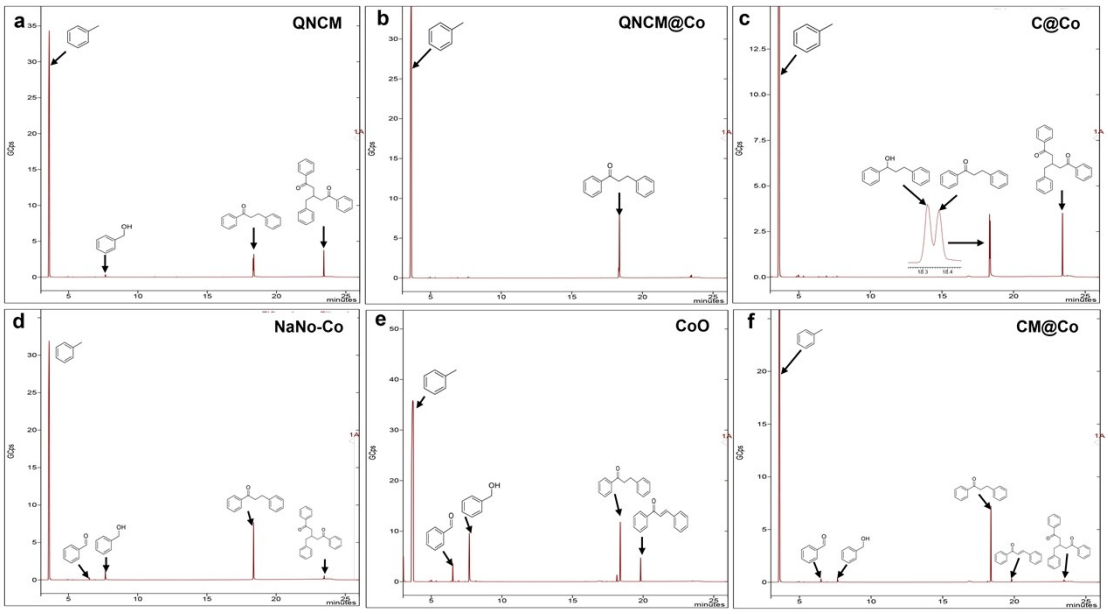

Figure S2. GC-MS Analysis for Comparing Catalyst Efficiency

5. Tables

Table S1. Elemental analysis testing of QNCM, QNCM@Co

Sample	Pore volume (cm^3/g)	Surface area (m^2/g)	Pore size (nm)
CCMQ	0.954	205.075	8.456
CoCCMQ	0.792	175.164	8.2743

Table S2. Some typical examples of the QNCM@Co catalyst and some reported heterogeneous or homogeneous catalysts

Catalyst	T (°C)	Catalyst amount (mol%)	Time (h)	Yield (%)	Number of substrates	TOF[a] (h^{-1})	References
LCN@Zn-SAC	110	1.5	4	92	26	15.33	*Nano Res.* **2022**, 15, 1874–1881
Co^{II}–PNP	120	2	24	93	26	1.93	*Org. Lett*. **2017**, 19, 1080–1083
Ni-Cat./L	140	5	36	94	33	0.52	*J. Org. Chem.* **2019**, 84, 769–779
Fe_3O_4@CS-Ni	110	3.98	7	90	16	3.23	*Appl Org Chem* **2022**, 36, e6838.
Co–MgO/TiO_2	110	17	20	95	14	0.28	*Catal. Sci. Technol.*, 2022, 12, 4113-4117
[IrCp*Cl_2]$_2$	40	2.5	20	76	19	1.52	*Chem. Eur. J.* **2018**, 24, 15529.
Cu(CH_3CN)4PF_6	75	2	24	94	15	1.95	*Monatsh Chem* **2017**, 152, 275–285
Co(II)-N	120	5	24	94	29	0.78	*Tetrahedron*, **2019**, 75: 130640.
nano-Fe_2O_3	135	3	24	97	12	1.35	*Chem. Commun*, **2019**, 55, 8490-8493
This Work	130	0.23	24	98	18	**17.75**	--

[a] TOF is calculated by following equation: $TOF = \frac{n_{product}}{t \times n_{catalyst}}$

6. Substrates

6.1 Ketones

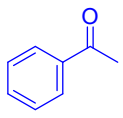

1a

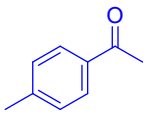

1b

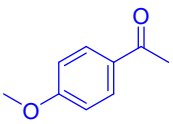

1c

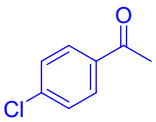

1d

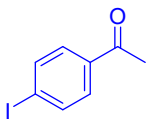

1e

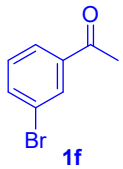

1f

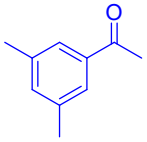

1g

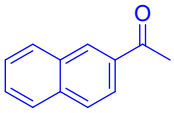

1h

1i

6.2 Alcohols

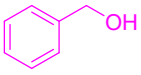

2a

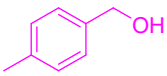

2b

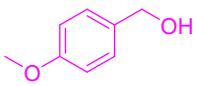

2c

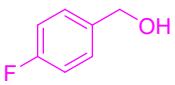

2d

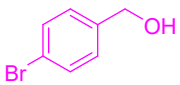

2e

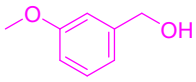

2f

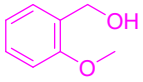

2g

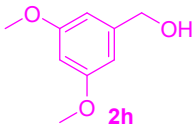

2h

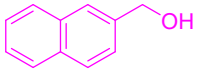

2i

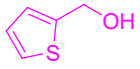

2j

7. General procedure for α-alkylation of ketones with alcohols

In a reaction flask equipped with a magnetic stirrer, were sequentially added aryl methyl ketone (0.2 mmol), alcohol (0.4 mmol), NaOH (0.2 mmol), and QNCM@Co (1.0 mg, 0.23 mol% of Co), followed by the addition of toluene (2 Ml) as a solvent. The mixture was heated to the target temperature in an oil bath while being stirred. Upon disappearance of the starting materials, the reaction mixture was cooled to room temperature and diluted with dichloromethane. The resulting mixture was filtered over a silica gel pad, and the filtrate was concentrated under reduced pressure. The residue was purified by column chromatography on silica gel to afford the α-alkylated product.

1,3-diphenylpropan-1-one (**3a**)

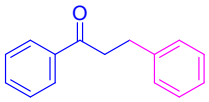

Proceeded at 130 ℃ for 24 h; purified by column chromatography on silica gel (using petroleum ether : EtOAc = 15 : 1 as an eluent); white solid; 41.1 mg, 98% yield.^{1}H NMR (400 MHz, $CDCl_3$) δ 7.95−7.83 (m, 2H), 7.53−7.33 (m, 3H), 7.27−7.09 (m, 5H), 3.23 (dd, *J* = 8.5, 6.9 Hz, 2H), 3.00 (dd, *J* = 8.5, 6.9 Hz, 2H). The data are consistent with those reported in the literature (*Tetrahedron,* **2019**, 75: 130640).

3-phenyl-1-(p-tolyl)propan-1-one (**3b**)

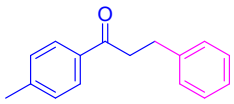

Proceeded at 130 ℃ for 24 h; purified by column chromatography on silica gel (using petroleum ether : EtOAc = 15 : 1 as an eluent); white solid;41.2 mg, 92% yield.^{1}H NMR (400 MHz, $CDCl_3$) δ 7.79 (d, *J* = 8.4 Hz, 2H), 7.23−7.07 (m, 9H), 3.21 (dd, *J* = 8.6, 6.8 Hz, 2H), 3.02−2.96 (m, 2H), 2.33 (s, 3H). The data are consistent with those reported in the literature (*Nano Res*. **2022**, 15, 1874–1881).

1-(4-methoxyphenyl)-3-phenylpropan-1-one (**3c**)

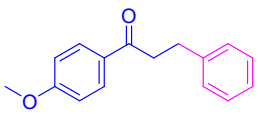

Proceeded at 130 °C for 24 h; purified by column chromatography on silica gel (using petroleum ether : EtOAc = 15 : 1 as an eluent); colorless liquid;42.2 mg, 88% yield.^{1}H NMR (400 MHz, $CDCl_3$) δ 7.92−7.85 (m, 2H), 7.24−7.13 (m, 5H), 6.90−6.82 (m, 2H), 3.78 (s, 3H), 3.21−3.13 (m, 2H), 3.03−2.94 (m, 2H). The data are consistent with those reported in the literature (*Nano Res*. **2022**, 15, 1874–1881).

1-(4-chlorophenyl)-3-phenylpropan-1-one (**3d**)

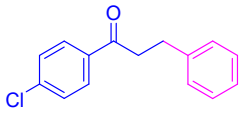

Proceeded at 130 °C for 24 h; purified by column chromatography on silica gel (using petroleum ether : EtOAc = 15 : 1 as an eluent); colorless liquid;42.5 mg, 87% yield.^{1}H NMR (400 MHz, $CDCl_3$) δ 7.84−7.77 (m, 2H), 7.35−7.31 (m, 2H), 7.22−7.13 (m, 5H), 3.18 (dd, *J* = 8.3, 6.7 Hz, 2H), 2.97 (t, *J* = 7.7 Hz, 2H). The data are consistent with those reported in the literature (*Appl Organomet Chem* **2022**, 36, e6838).

1-(4-iodophenyl)-3-phenylpropan-1-one (**3e**)

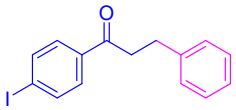

Proceeded at 130 °C for 24 h; purified by column chromatography on silica gel (using petroleum ether : EtOAc = 15 : 1 as an eluent); yellow liquid;57.7 mg, 86% yield.^{1}H NMR (400 MHz, $CDCl_3$) δ 7.80−7.71 (m, 2H), 7.62−7.55 (m, 2H), 7.23−7.15 (m, 5H), 3.23−3.15 (m, 2H), 3.03−2.93 (m, 2H). The data are consistent with those reported in the literature (*Chem. Eur. J.* **2018**, 24, 15529).

1-(3-bromophenyl)-3-phenylpropan-1-one (**3f**)

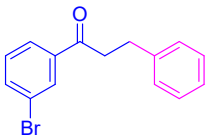

Proceeded at 130 °C for 24 h; purified by column chromatography on silica gel (using petroleum ether : EtOAc = 15 : 1 as an eluent); yellow liquid;46.6 mg, 81% yield.^{1}H NMR (400 MHz, $CDCl_3$) δ 7.90−7.82 (m, 2H), 7.51−7.44 (m, 1H), 7.40−7.29 (m, 4H),

7.25 (dd, *J* = 8.6, 2.2 Hz, 1H), 7.07−7.00 (m, 2H), 3.19 (t, *J* = 7.5 Hz, 2H), 2.95 (q, *J* = 7.0 Hz, 2H). The data are consistent with those reported in the literature (*Monatsh Chem* **2021**, 152, 275–285).

1-(3,5-dimethylphenyl)-3-phenylpropan-1-one (**3g**)

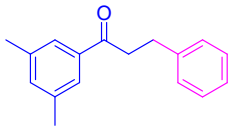

Proceeded at 130 ℃ for 24 h; purified by column chromatography on silica gel (using petroleum ether : EtOAc = 15 : 1 as an eluent); colorless liquid;43.0 mg, 90% yield.^{1}H NMR (400 MHz, $CDCl_3$) δ 7.55 (d, *J* = 14.9 Hz, 2H), 7.31−7.17 (m, 6H), 3.28 (t, *J* = 7.8 Hz, 2H), 3.05 (t, J = 7.8 Hz, 2H), 2.36 (s, 6H). The data are consistent with those reported in the literature (*Org. Lett.* **2017**, 19, 5, 1080–1083).

1-(naphthalen-2-yl)-3-phenylpropan-1-one (**3h**)

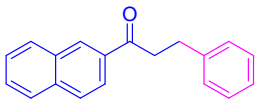

Proceeded at 130 ℃ for 24 h; purified by column chromatography on silica gel (using petroleum ether : EtOAc = 15 : 1 as an eluent); white solid;46.2 mg, 89% yield.^{1}H NMR (400 MHz, $CDCl_3$) δ 7.83−7.76 (m, 3H), 7.72 (s, 1H), 7.44 (ddd, *J* = 10.3, 5.9, 1.8 Hz, 3H), 7.30−7.23 (m, 2H), 7.21−7.14 (m, 3H), 2.79−2.59 (m, 2H), 2.22−2.08 (m, 2H). The data are consistent with those reported in the literature (*Chem. Eur. J.* **2018**, 24, 15529).

3-phenyl-1-(quinolin-6-yl)propan-1-one (**3i**)

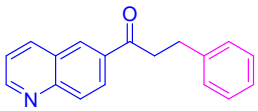

Proceeded at 130 ℃ for 24 h; purified by column chromatography on silica gel (using petroleum ether : EtOAc = 15 : 1 as an eluent); yellow solid;42.8 mg, 82% yield.^{1}H NMR (400 MHz, $CDCl_3$) δ 8.70 (dd, *J* = 4.3, 1.8 Hz, 1H), 7.98 (dd, *J* = 25.2, 8.4 Hz, 2H), 7.58−7.50 (m, 2H), 7.40−7.23 (m, 6H), 3.00−2.79 (m, 2H), 2.28−2.05 (m, 2H).

The data are consistent with those reported in the literature (*Org. Lett.* **2017**, 19, 5, 1080–1083).

1-phenyl-3-(p-tolyl)propan-1-one (**3j**)

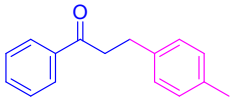

Proceeded at 130 ℃ for 24 h; purified by column chromatography on silica gel (using petroleum ether : EtOAc = 15 : 1 as an eluent); white solid;40.7 mg, 91% yield.^{1}H NMR (400 MHz, $CDCl_3$) δ 7.98−7.90 (m, 2H), 7.57−7.50 (m, 1H), 7.46−7.39 (m, 2H), 7.12 (q, *J* = 8.1 Hz, 4H), 3.30−3.22 (m, 2H), 3.05−2.98 (m, 2H), 2.31 (s, 3H). The data are consistent with those reported in the literature (*Tetrahedron,* **2019**, 75: 130640).

3-(4-methoxyphenyl)-1-phenylpropan-1-one (**3k**)

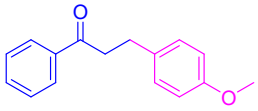

Proceeded at 130 ℃ for 24 h; purified by column chromatography on silica gel (using petroleum ether : EtOAc = 15 : 1 as an eluent); colorless liquid;43.2 mg, 90% yield.^{1}H NMR (400 MHz, $CDCl_3$) δ 7.97−7.90 (m, 2H), 7.57−7.50 (m, 1H), 7.47−7.40 (m, 2H), 7.16 (d, *J* = 8.6 Hz, 2H), 6.83 (d, *J* = 8.7 Hz, 2H), 3.77 (s, 3H), 3.29−3.21 (m, 2H), 3.04−2.96 (m, 2H). The data are consistent with those reported in the literature (*Catal. Sci. Technol.*, **2022**, 12, 4113-4117).

3-(4-fluorophenyl)-1-phenylpropan-1-one (**3l**)

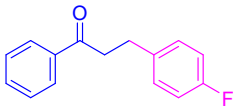

Proceeded at 130 ℃ for 24 h; purified by column chromatography on silica gel (using petroleum ether : EtOAc = 15 : 1 as an eluent); yellow liquid;40.5 mg, 89% yield.^{1}H NMR (400 MHz, $CDCl_3$) δ 7.91−7.79 (m, 2H), 7.44 (t, *J* = 7.4 Hz, 1H), 7.34 (t, *J* = 7.7 Hz, 2H), 7.17−7.03 (m, 2H), 6.86 (t, *J* = 8.7 Hz, 2H), 3.16 (t, *J* = 7.6 Hz, 2H), 2.93 (t, *J* = 7.6 Hz, 2H). The data are consistent with those reported in the literature (*Org. Lett.* **2017**, 19, 5, 1080–1083).

3-(4-bromophenyl)-1-phenylpropan-1-one (**3m**)

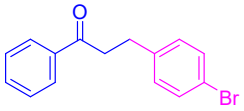

Proceeded at 130 ℃ for 24 h; purified by column chromatography on silica gel (using petroleum ether : EtOAc = 15 : 1 as an eluent); yellow liquid;48.9 mg, 85% yield.^{1}H NMR (400 MHz, $CDCl_3$) δ 7.90−7.82 (m, 2H), 7.51−7.44 (m, 1H), 7.40−7.29 (m, 4H), 7.25 (dd, *J* = 8.6, 2.2 Hz, 1H), 7.07−7.00 (m, 2H), 3.19 (t, *J* = 7.5 Hz, 2H), 2.95 (q, *J* = 7.0 Hz, 2H). The data are consistent with those reported in the literature (*Nano Res*. **2022**, 15, 1874–1881).

3-(3-methoxyphenyl)-1-phenylpropan-1-one (**3n**)

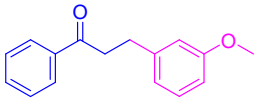

Proceeded at 130 ℃ for 24 h; purified by column chromatography on silica gel (using petroleum ether : EtOAc = 15 : 1 as an eluent); white solid;39.8 mg, 83% yield.^{1}H NMR (400 MHz, $CDCl_3$) δ 8.01−7.89 (m, 2H), 7.60−7.50 (m, 1H), 7.44 (t, *J* = 7.6 Hz, 2H), 7.27−7.16 (m, 1H), 6.87−6.70 (m, 3H), 3.78 (s, 3H), 3.32−3.23 (m, 2H), 3.10−2.99 (m, 2H). The data are consistent with those reported in the literature (*J. Org. Chem.* **2019**, 84, 2, 769–779).

3-(2-methoxyphenyl)-1-phenylpropan-1-one (**3o**)

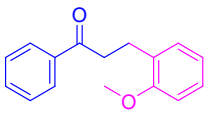

Proceeded at 130 ℃ for 24 h; purified by column chromatography on silica gel (using petroleum ether : EtOAc = 15 : 1 as an eluent); colorless liquid;40.8 mg, 85% yield.^{1}H NMR (400 MHz, $CDCl_3$) δ 7.97 (d, *J* = 8.0 Hz, 2H), 7.53 (t, *J* = 7.4 Hz, 1H), 7.46−7.39 (m, 2H), 7.25−7.16 (m, 2H), 6.92−6.82 (m, 2H), 3.81 (s, 3H), 3.29−3.22 (m, 2H), 3.08−3.01 (m, 2H). The data are consistent with those reported in the literature (*Catal. Sci. Technol.*, **2022**, 12, 4113-4117).

3-(3,5-dimethoxyphenyl)-1-phenylpropan-1-one (**3p**)

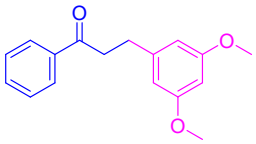

Proceeded at 130 ℃ for 24 h; purified by column chromatography on silica gel (using petroleum ether : EtOAc = 15 : 1 as an eluent); white solid;43.7 mg, 81% yield.^{1}H NMR (400 MHz, $CDCl_3$) δ 7.99−7.92 (m, 2H), 7.55 (t, *J* = 7.4 Hz, 1H), 7.45 (t, *J* = 7.7 Hz, 2H), 6.41 (d, *J* = 2.2 Hz, 2H), 6.32 (t, *J* = 2.3 Hz, 1H), 3.77 (s, 6H), 3.34−3.23 (m, 2H), 3.05−2.95 (m, 2H). The data are consistent with those reported in the literature (*Nano Res*. **2022**, 15, 1874–1881).

3-(naphthalen-2-yl)-1-phenylpropan-1-one (**3q**)

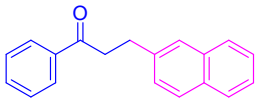

Proceeded at 130 ℃ for 24 h; purified by column chromatography on silica gel (using petroleum ether : EtOAc = 15 : 1 as an eluent); white solid;46.8 mg, 90% yield.^{1}H NMR (400 MHz, $CDCl_3$) δ 7.98−7.90 (m, 2H), 7.76 (t, *J* = 8.2 Hz, 3H), 7.65 (d, *J* = 1.8 Hz, 1H), 7.55−7.48 (m, 1H), 7.46−7.33 (m, 5H), 3.37−3.30 (m, 2H), 3.24−3.16 (m, 2H). The data are consistent with those reported in the literature (*Tetrahedron,* **2019**, 75: 130640).

1-phenyl-3-(thiophen-2-yl)propan-1-one (**3r**)

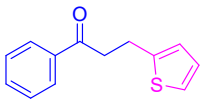

Proceeded at 130 ℃ for 24 h; purified by column chromatography on silica gel (using petroleum ether : EtOAc = 15 : 1 as an eluent); yellow solid;35.4 mg, 82% yield.^{1}H NMR (400 MHz, $CDCl_3$) δ 7.40−7.25 (m, 5H), 7.11 (d, *J* = 5.1 Hz, 1H), 6.91 (dd, *J* = 5.1, 3.4 Hz, 1H), 6.79 (d, *J* = 2.4 Hz, 1H), 2.98−2.84 (m, 2H), 2.18−2.03 (m, 2H). The data are consistent with those reported in the literature (*Nano Res*. **2022**, 15, 1874–1881).

8. Supplementary discussion

8.1 Specific surface area

In the specific surface area analysis, the results showed that the pore volume of QNCM decreases after Co loading, especially in the mesoporous region (about 16 nm). This change is mainly due to that the penetration of cobalt ions fills up part of the pores in the material, resulting in the decrease of specific surface area.

8.2 large Co particles

QNCM@Co contains a small number of relatively large Co particles. To determine the composition of these larger particles, XRD analysis on QNCM@Co and commercial nano-cobalt oxide (CoO) was performed (Figure S3). The results show that QNCM@Co exhibits a distinct cobalt oxide (111) diffraction peak. Further activity tests indicate that the catalytic activity of commercial nano-cobalt oxide is significantly lower than that of QNCM@Co. It can be inferred that these larger particles are mainly nano cobalt oxide formed by the aggregation of some cobalt during the activation process and are not the main active sites in the α-alkylation reaction. In the QNCM@Co catalyzed α-alkylation of ketones with alcohols, the truly active sites are the tiny cobalt nanoparticles coordinated to N/O, rather than the larger cobalt oxide clusters.

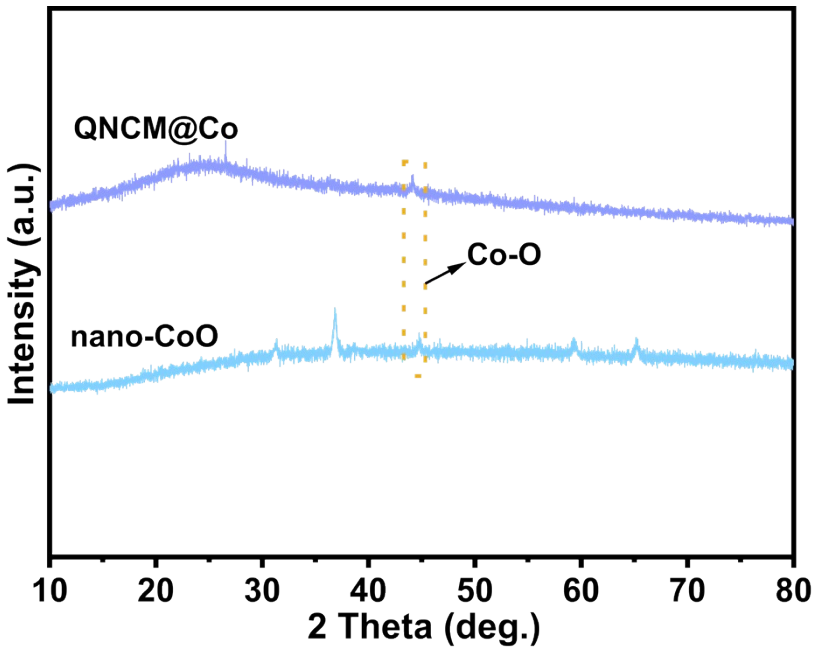

Figure S3. XRD spectra of nano-CoO and QNCM@Co

8.3 Reaction conditions

8.3.1 Solvent

Toluene was selected as the optimal solvent based on a combination of various factors. 1) With regard to solvent polarity, toluene, as a nonpolar solvent, can effectively dissolve hydrophobic substrates while minimizing competitive adsorption at the catalyst's active sites. In contrast, polar solvents (such as DMF, which yields a conversion rate of only 5%) tend to form weak coordination bonds with cobalt nanoparticles, potentially occupying some of the active sites and inhibiting the catalytic reaction. 2) Regarding the boiling point, the optimal temperature for this reaction is 130°C. Since toluene has a boiling point of 110°C, stable reflux conditions can be maintained at this temperature to ensure the reaction proceeds smoothly. Conversely, low boiling point solvents (such as dichloromethane and *n*-hexane, whose yields are only 10% and 27%, respectively) are highly volatile, which is difficult to meet the temperature requirements of the reaction system.

8.3.2 Base

NaOH performs exceptionally well in this reaction, primarily due to the optimal balance between its basicity and cationic effects. In the α-alkylation reaction of ketones with benzyl alcohol, the role of the base is primarily manifested in two key aspects: 1) It promotes the deprotonation of the hydroxyl group on benzyl alcohol to form the benzylmethoxyl anion. 2) It boosts the reduction of the C=C bond. The reaction proceeds smoothly and yields the desired product, 1,3-diphenylpropan-1-one (**3a**), only when the strength of the base is appropriate. If the base is too weak, it cannot deprotonate the hydroxyl group of benzyl alcohol, thereby hindering the catalyst's ability to dehydrogenate the benzylmethoxyl anion to form benzaldehyde. For example, the weak base K_2CO_3 and triethylamine are unable to effectively strip proton, resulting in a yield of only 11–15%; If the base is too strong, the target product **3a** is easily reduced further to the byproduct 1,3-diphenylpropan-1-ol. For example, the strong base KOtBu is easy to lead to excessive reduction to produce 1,3-diphenyl-1-propanol (see Figure S4 after GC-MS analysis), and the yield is 76%. Therefore, the excellent performance of NaOH in this α-alkylation reaction is primarily due to its good compatibility with the reaction steps.

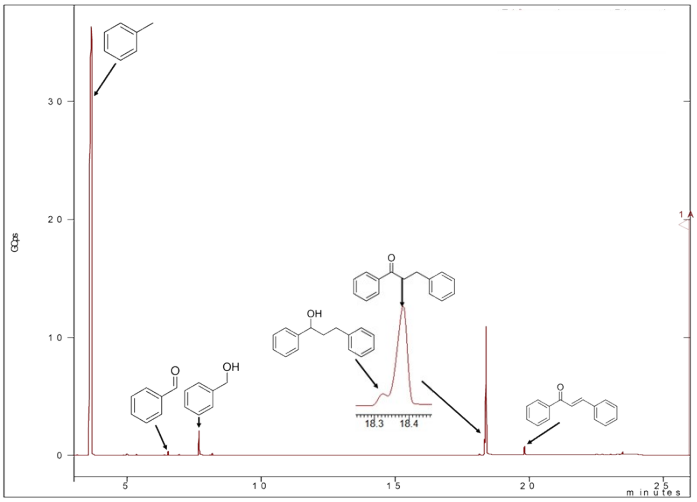

Figure S4. GC-MS analysis using the strong base KOtBu

8.3.3 Amount of NaOH

The yield of product 3a was 98% when the amount of NaOH is 0.2 mmol; when the amount of NaOH is further increased, the yield decreases slightly. This suggests that an increase in the amount of base may cause the target product **3a** to undergo further reduction to form 1,3-diphenylpropane-1-ol, thereby leading to a decrease in the yield. As shown in Figure S5, when the amount of sodium hydroxide reached 0.4 mmol, the yield dropped to only 62%; GC-MS analysis confirmed the formation of 1,3-diphenylpropan-1-ol.

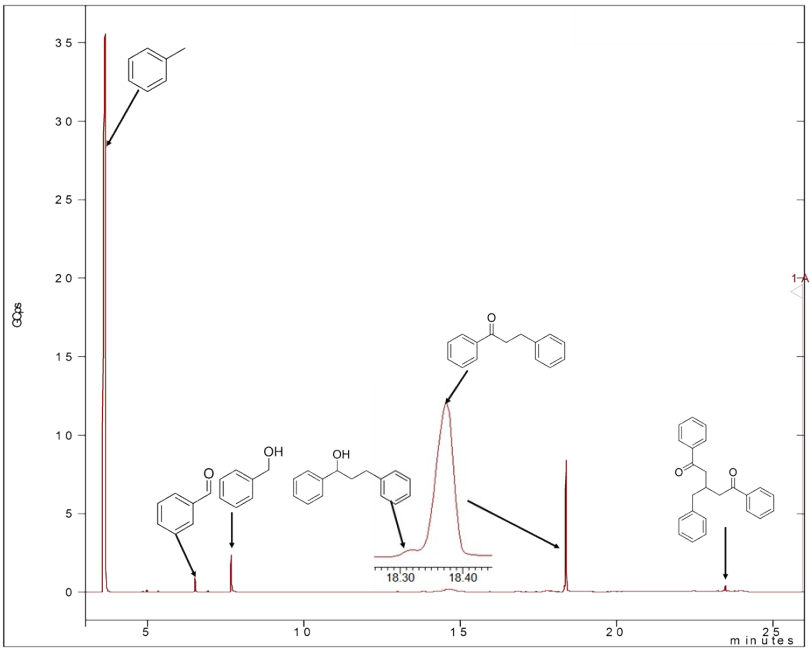

Figure S5. GC-MS analysis of the reaction using 0.4 mmol of NaOH

8.3.4 Temperature

The reaction is kinetically controlled, the yield increases as the temperature rises below 130°C. Above this temperature, the yield decreases because excessive heat causes the target product to undergo over-reduction; as shown in Figure S6, the yield of the target product drops significantly at 140°C, and GC-MS analysis indicates that it is primarily reduced to 1,3-diphenyl-1-propanol. We have incorporated this data into the revised manuscript.

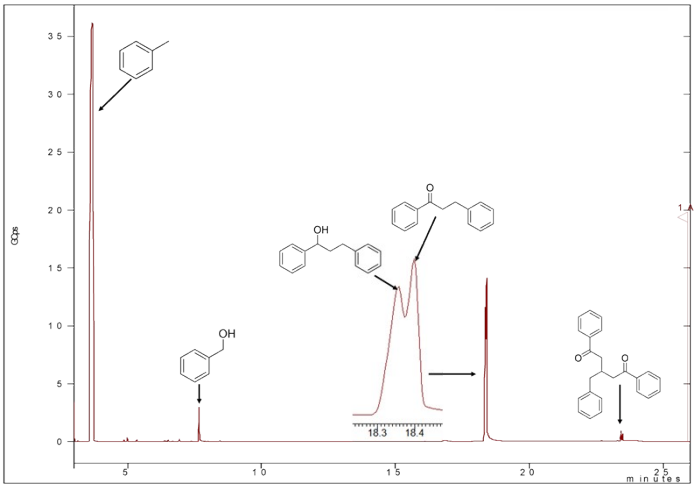

Figure S6. GC-MS analysis of the reaction at 140 °C

8.3.5 Electron effects in substrate scope

In the α-alkylation reaction of ketones with alcohols, the reaction process primarily consists of the following three steps. 1. Benzene-1-ol 2a is oxidized to form benzaldehyde, while the α-H of benzene-1-ol 2a is transferred to the metal center of the catalyst, thereby forming a metal hydride (M−H). 2. benzaldehyde reacts with acetophenone 1a, and then dehydrates to form chalcone intermediate. 3. The M−H group selectively reduces the C=C bond of the chalcone intermediate to yield the target product, 1,3-diphenyl-1-propanone 3a, thereby completing the catalytic cycle. In the oxidation of benzyl alcohol to benzaldehyde, electron-donating groups can increase the electron density at the hydroxyl group of benzyl alcohol, thereby promoting the oxidation reaction. In Step 3, during the reduction of the C=C double bond in the chalcone intermediate, the electron-donating group stabilizes the C=C double bond, thereby hindering the reduction reaction. Electron-withdrawing groups reduce the electron density at the hydroxyl group of benzyl alcohol, thereby inhibiting the oxidation reaction; however, during the selective reduction of the chalcone intermediate, electron-withdrawing groups reduce the electron density at the C=C double bond, promoting the reduction reaction. Nevertheless, because the oxidation of benzyl alcohol is a rate limiting step in the whole reaction, the yield of electron withdrawing group is slightly lower than that of electron donating group. Thus, it appears to be no significant difference in the yields of substrates containing electron-donating and electron-withdrawing groups in the α-alkylation of ketones and alcohols.

9. NMR spectra

^{1}H NMR spectrum for compound 3a

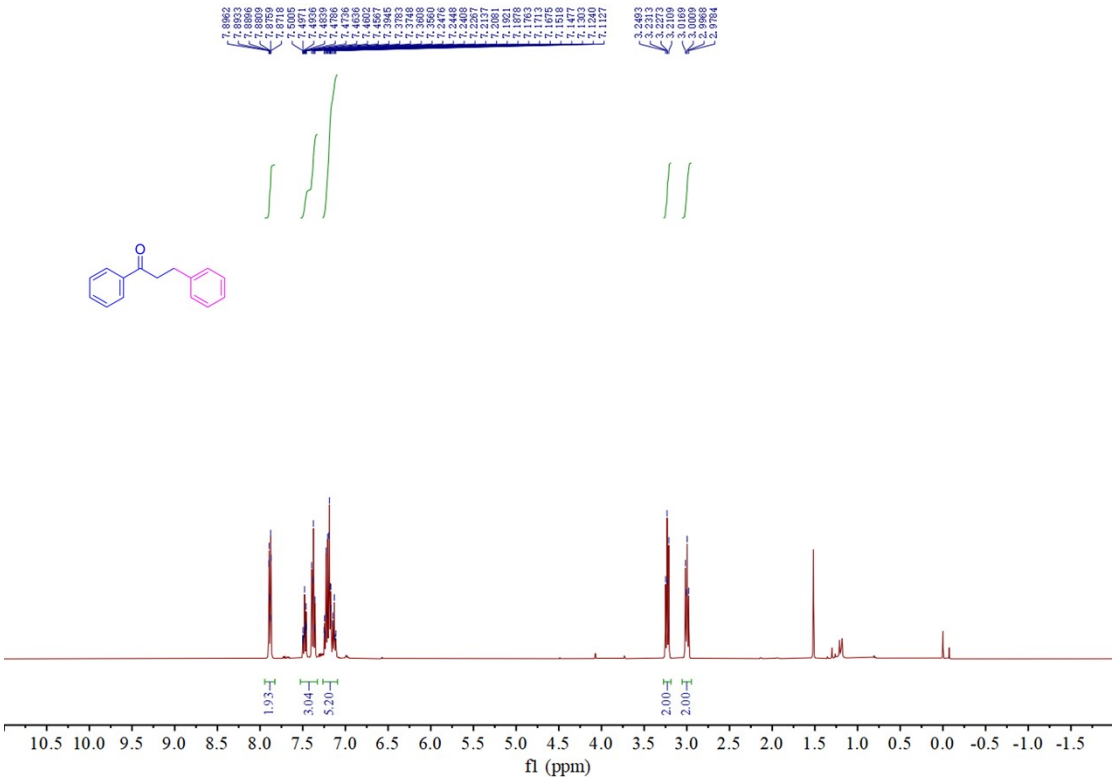

^{1}H NMR spectrum for compound 3b

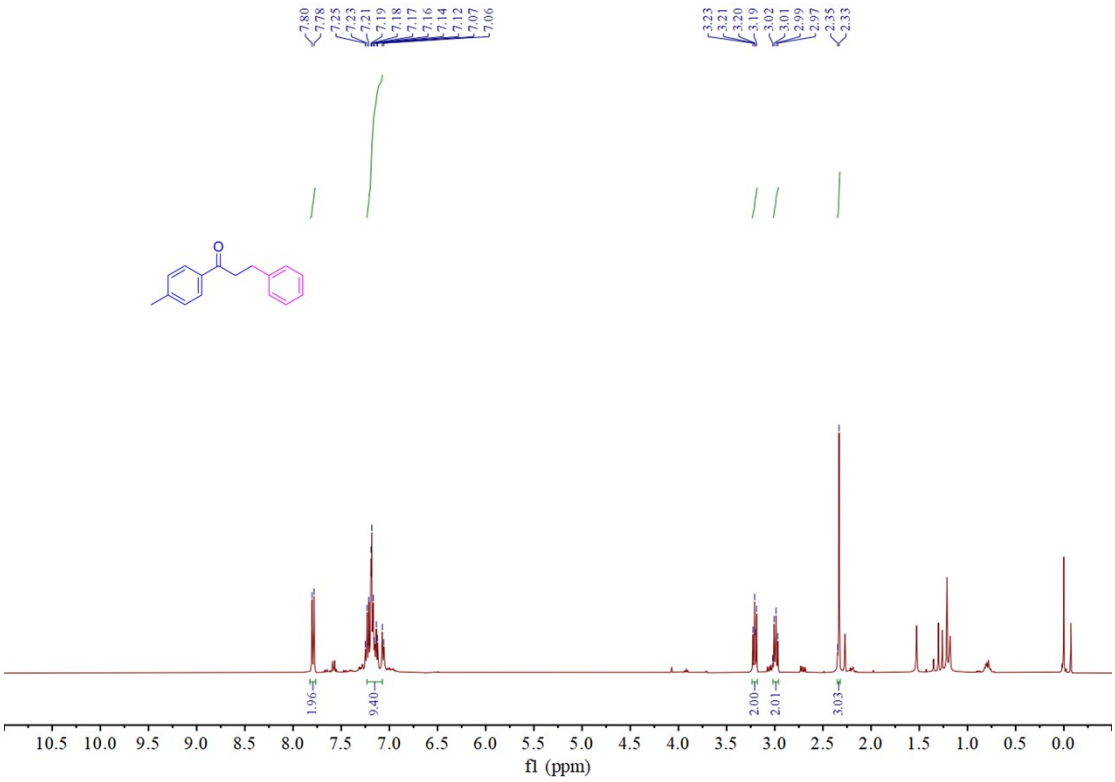

^{1}H NMR spectrum for compound 3c

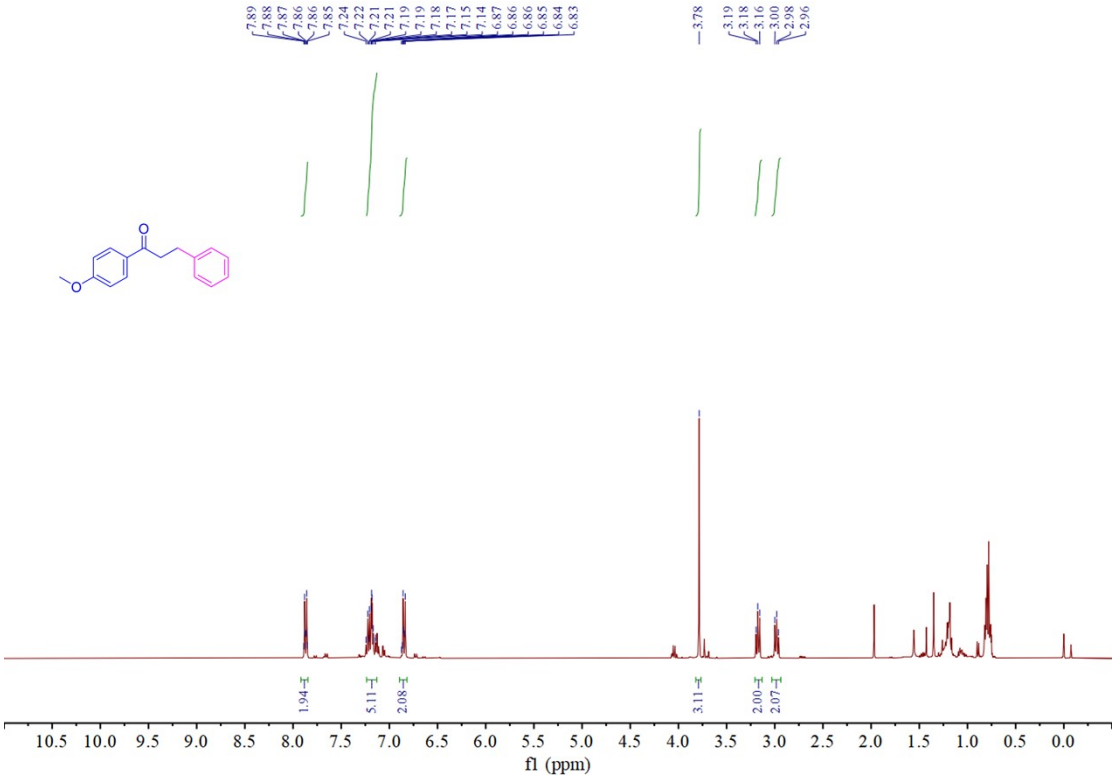

^{1}H NMR spectrum for compound 3d

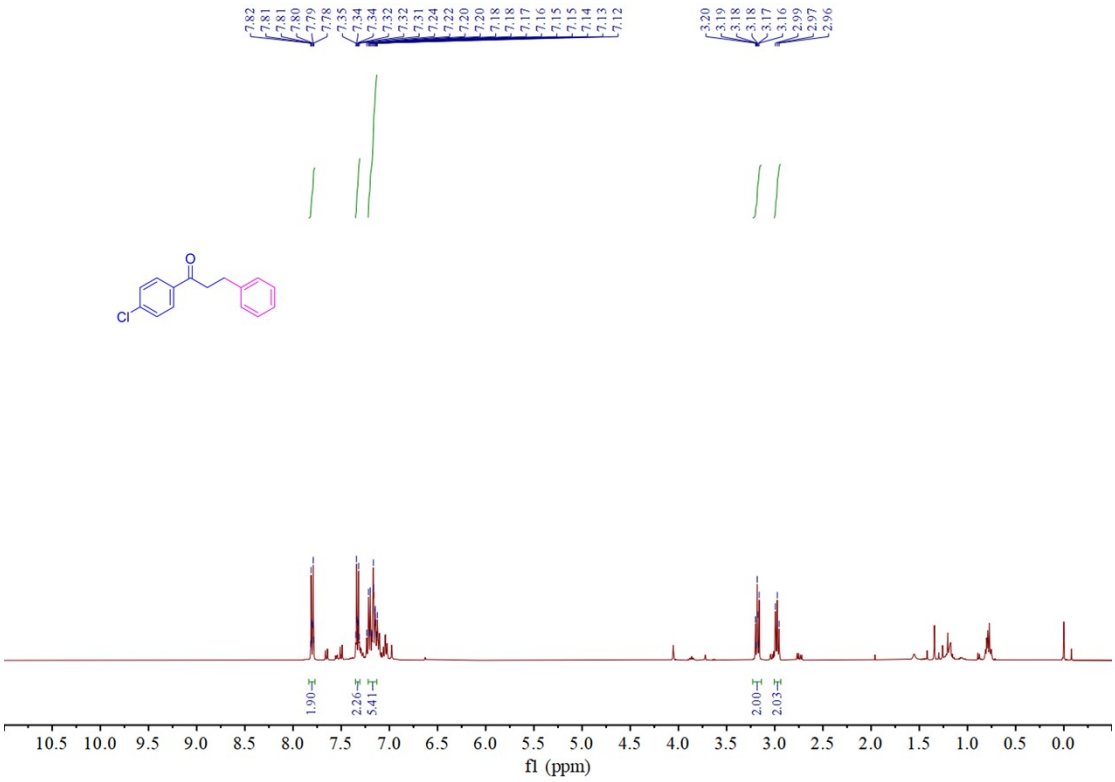

^{1}H NMR spectrum for compound 3e

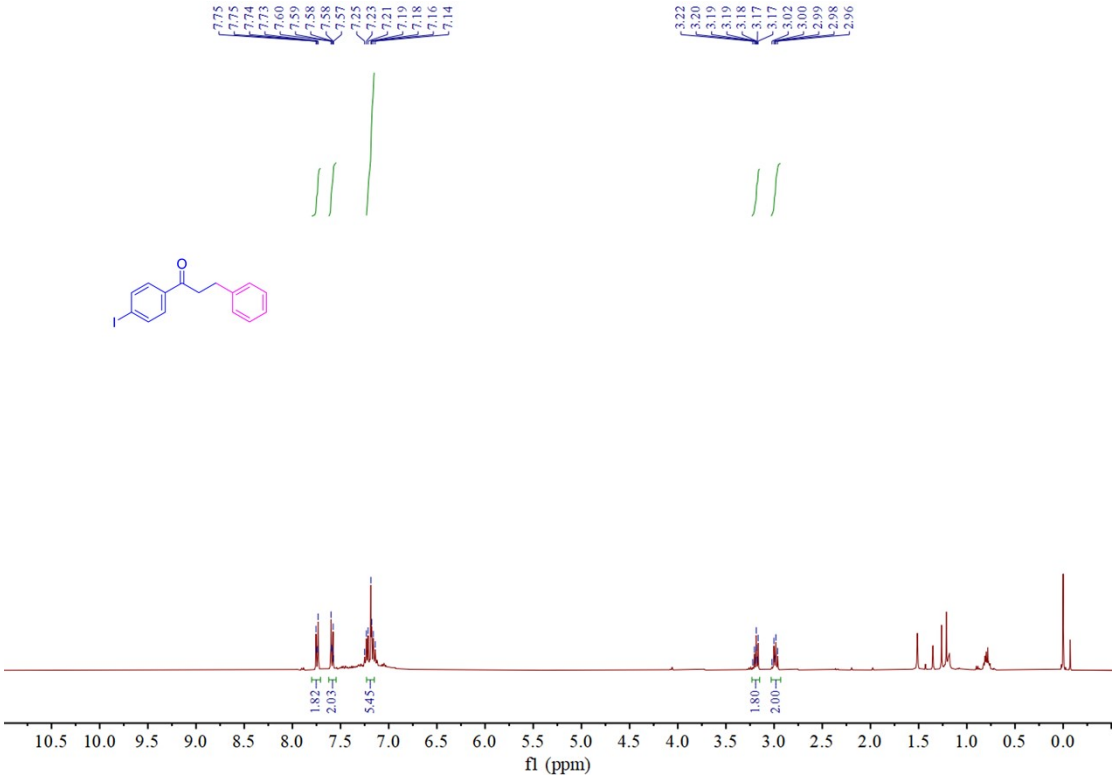

^{1}H NMR spectrum for compound 3f

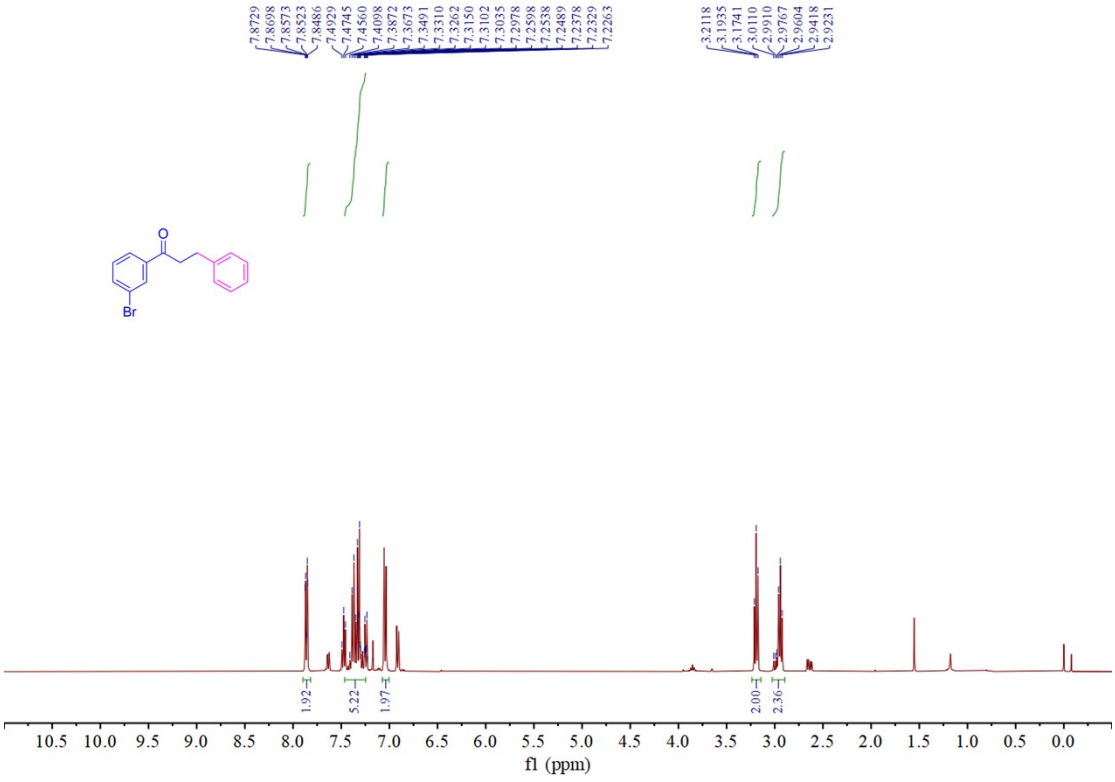

^{1}H NMR spectrum for compound 3g

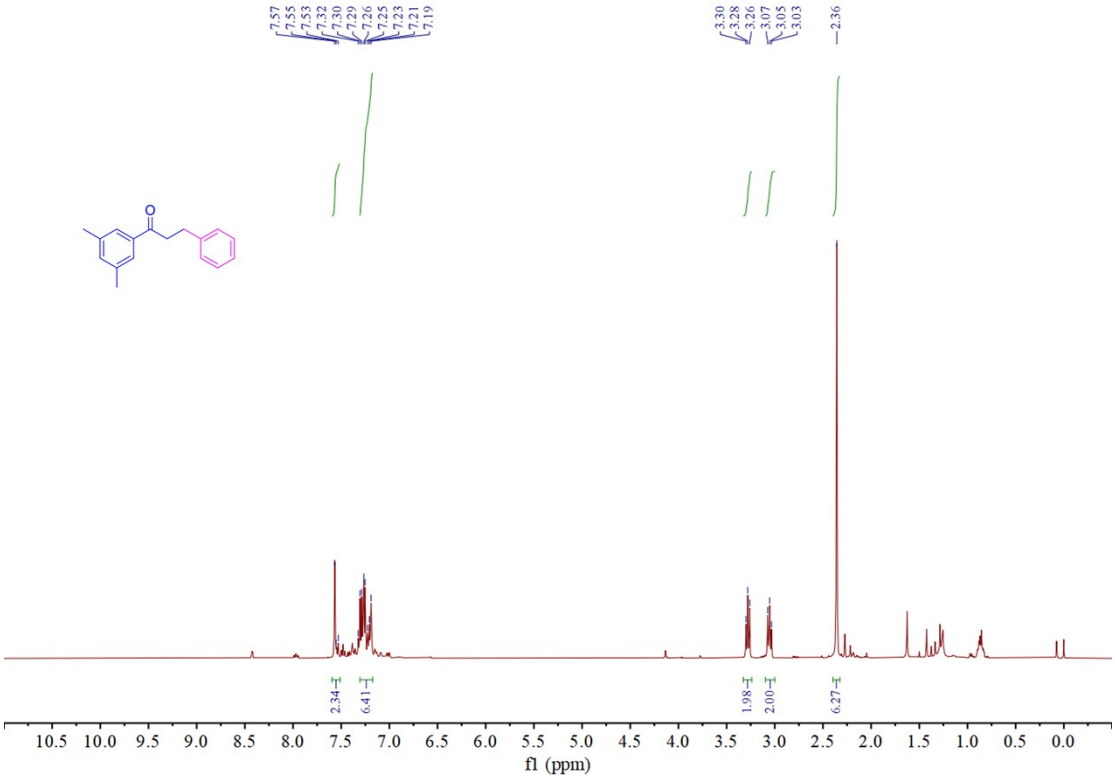

^{1}H NMR spectrum for compound 3h

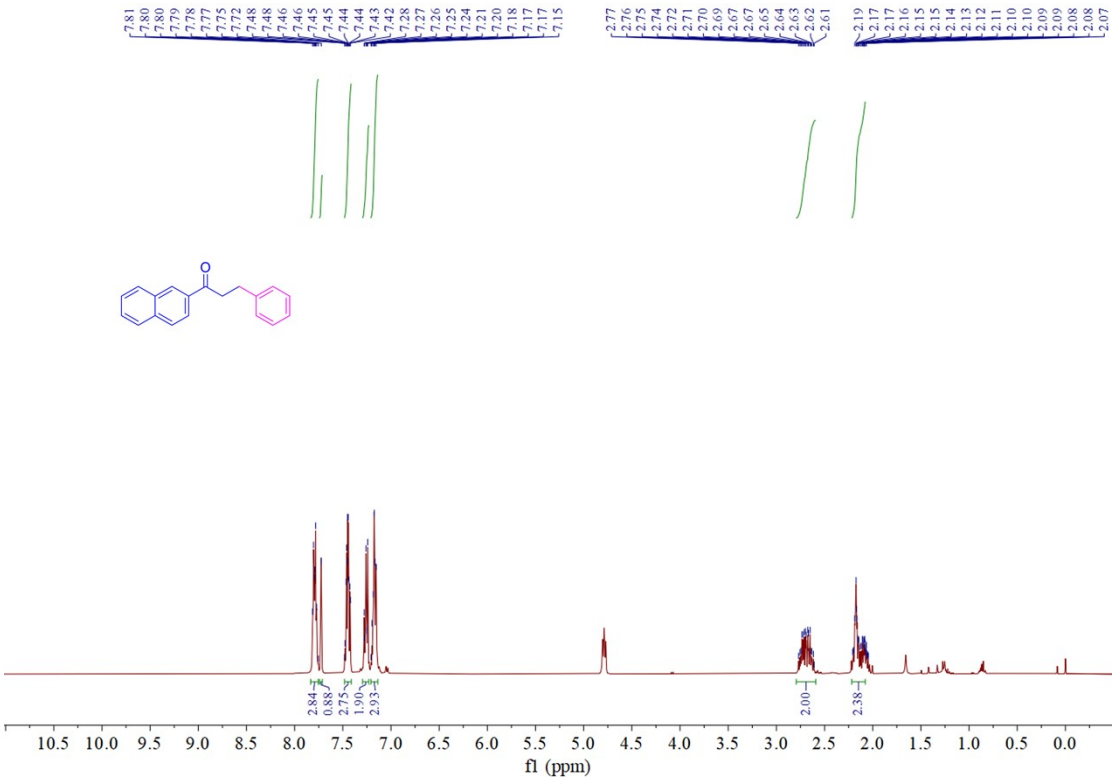

^{1}H NMR spectrum for compound 3i

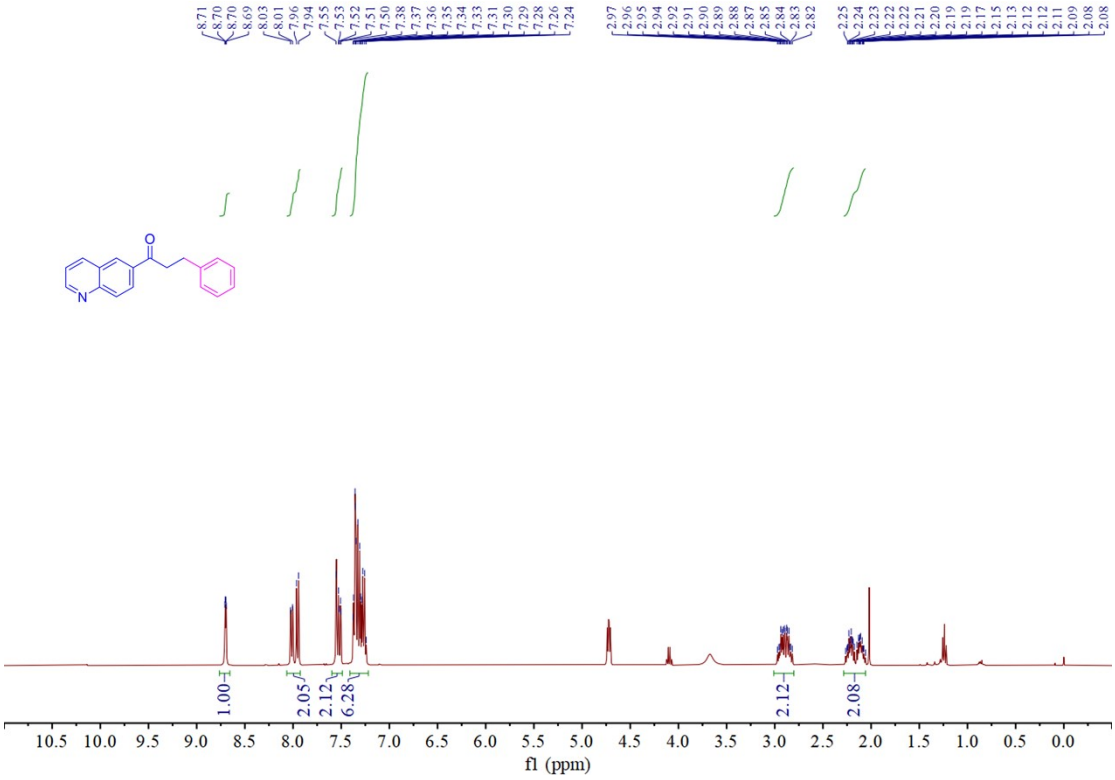

^{1}H NMR spectrum for compound 3j

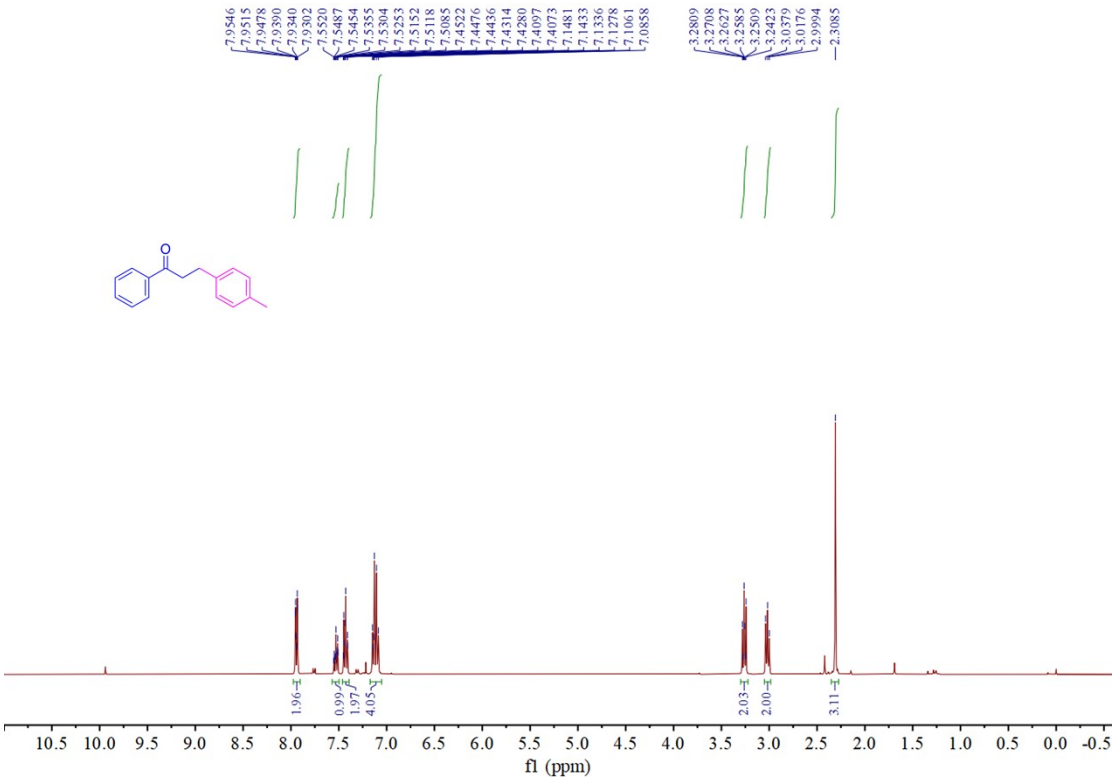

^{1}H NMR spectrum for compound 3k

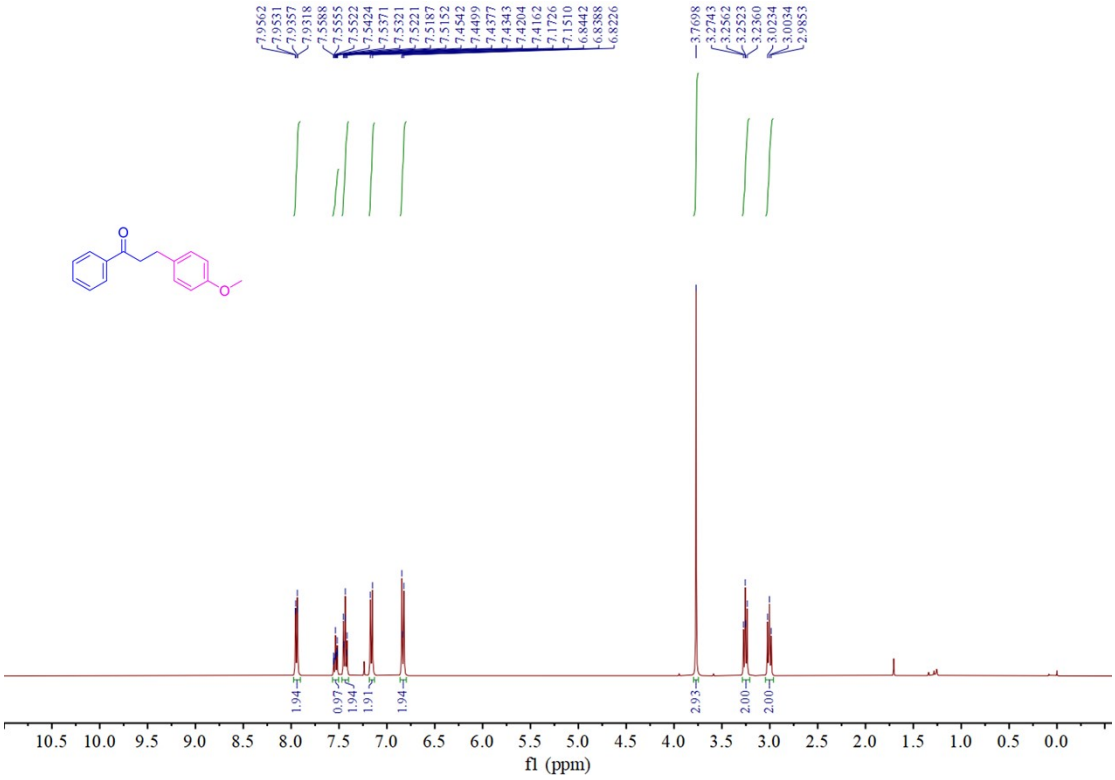

^{1}H NMR spectrum for compound 3l

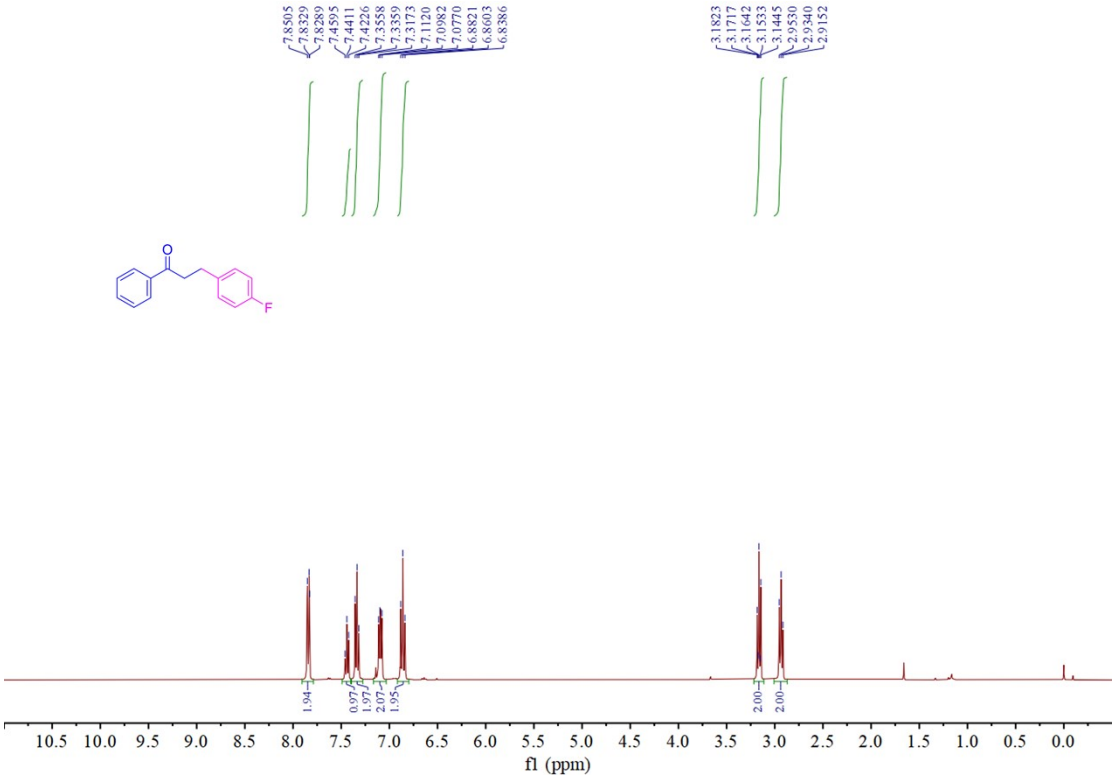

^{1}H NMR spectrum for compound 3m

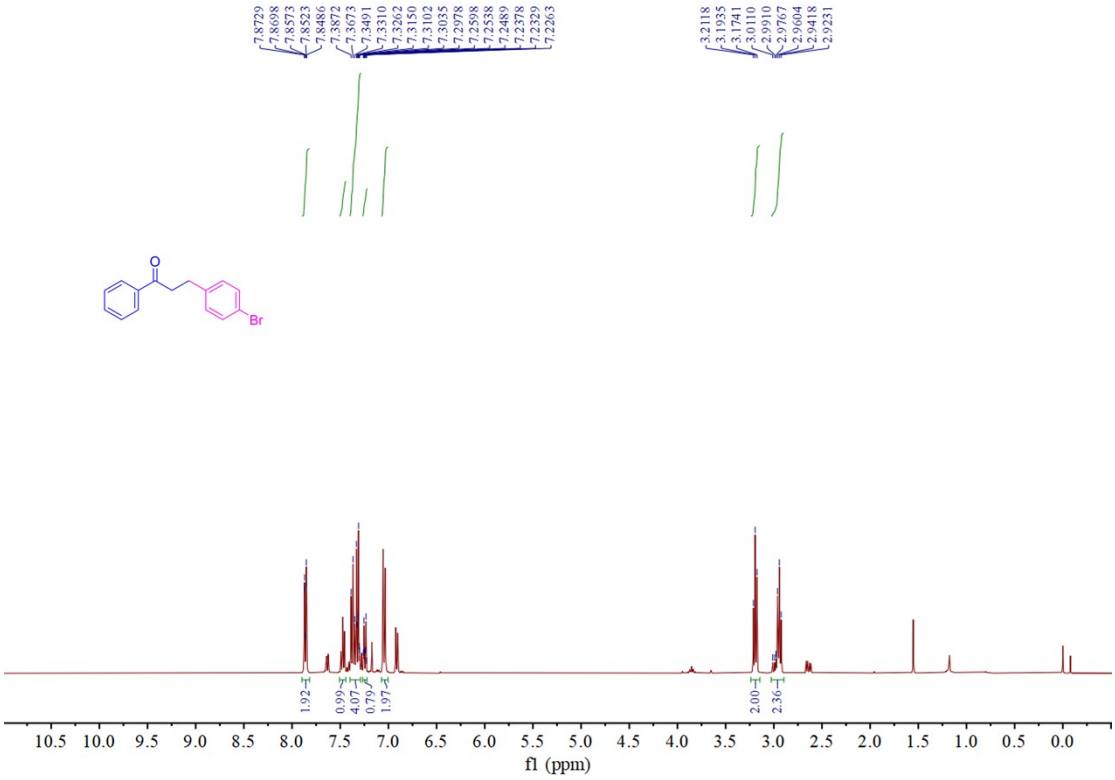

^{1}H NMR spectrum for compound 3n

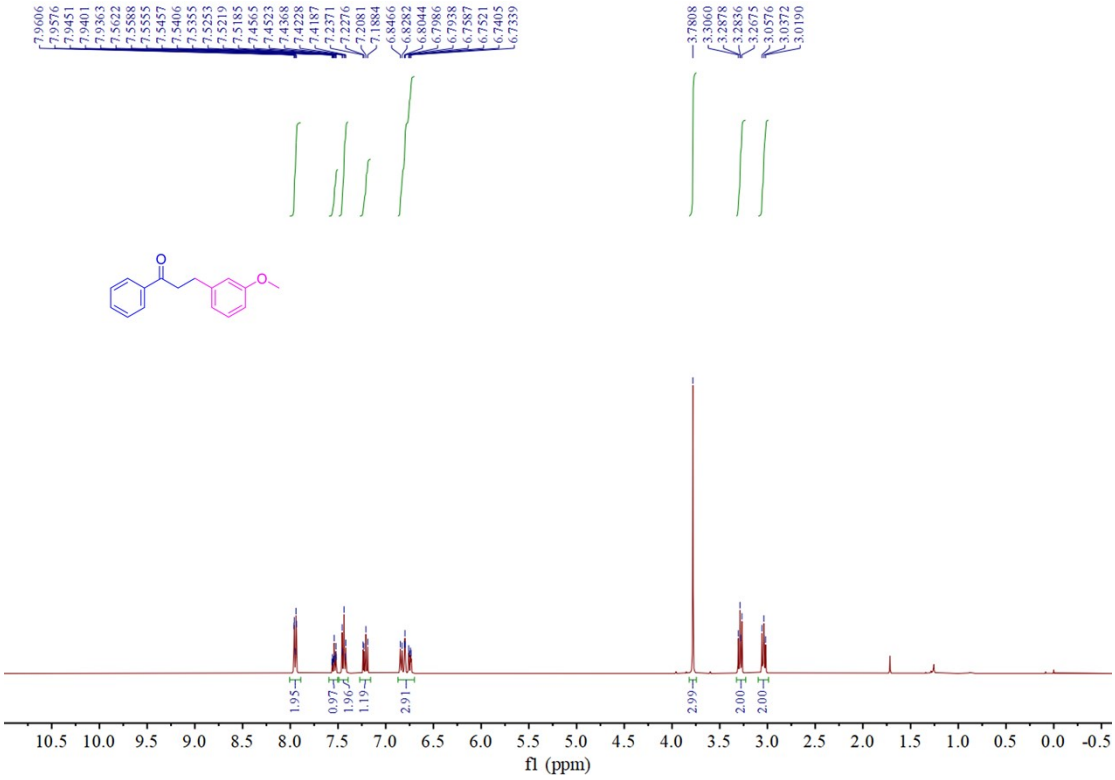

^{1}H NMR spectrum for compound 3o

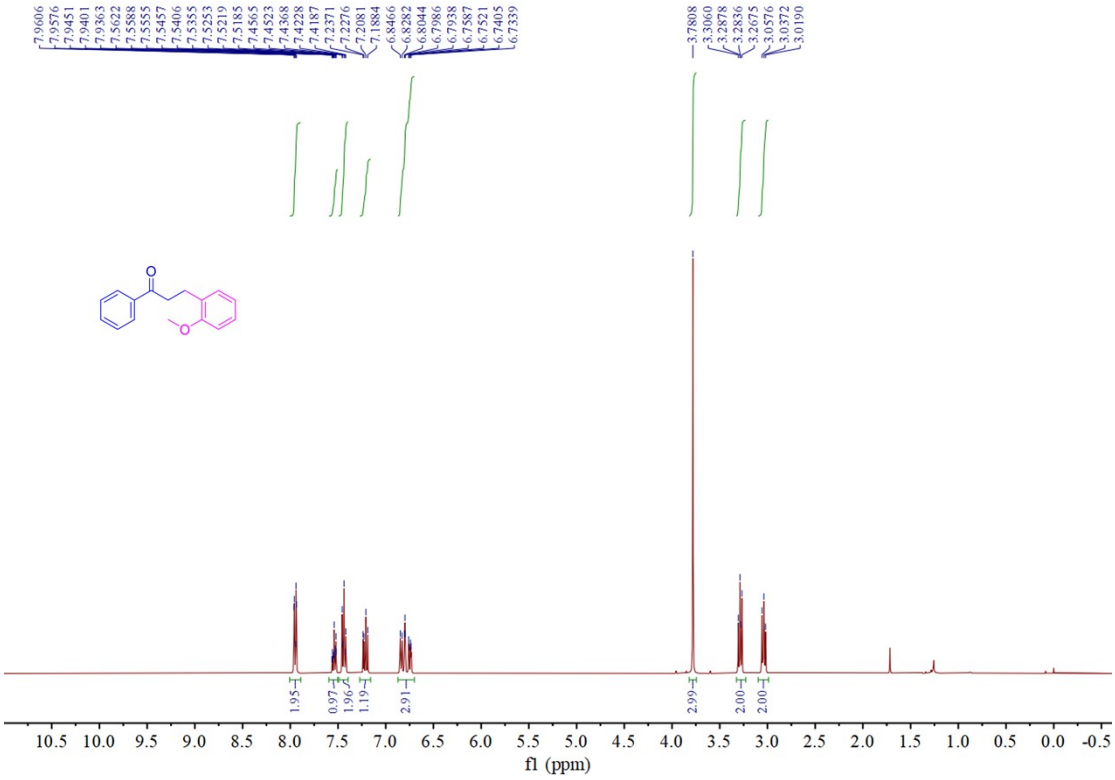

^{1}H NMR spectrum for compound 3p

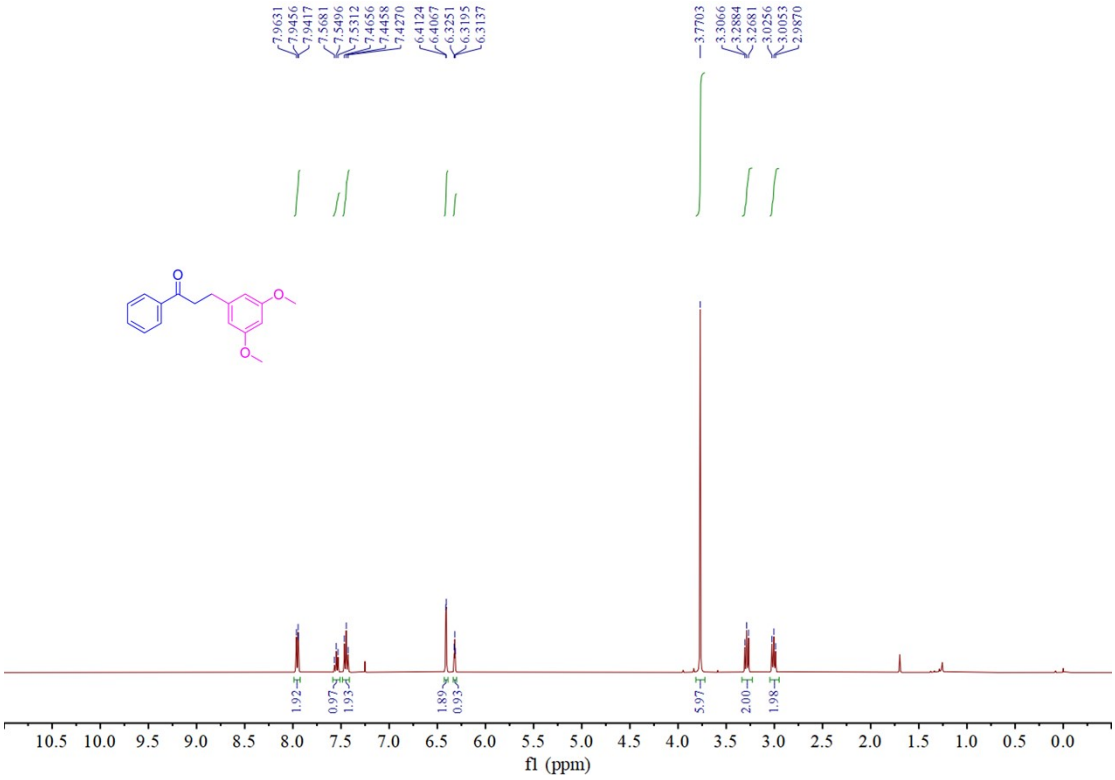

^{1}H NMR spectrum for compound 3q

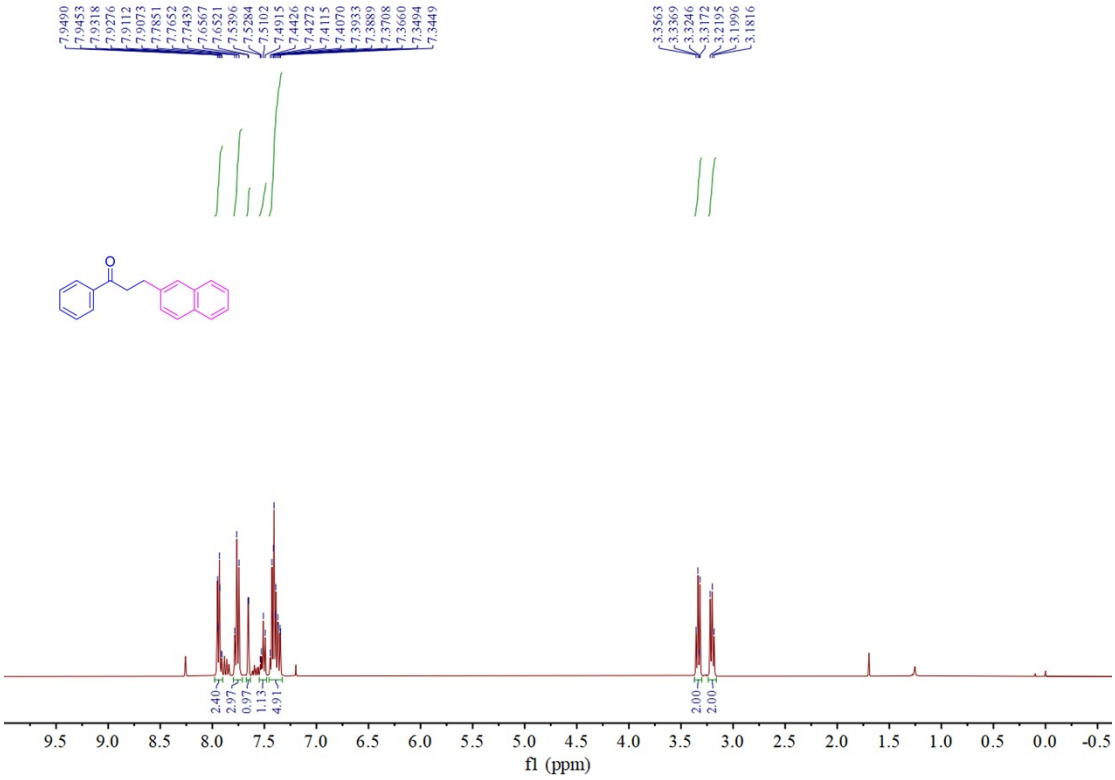

^{1}H NMR spectrum for compound 3r

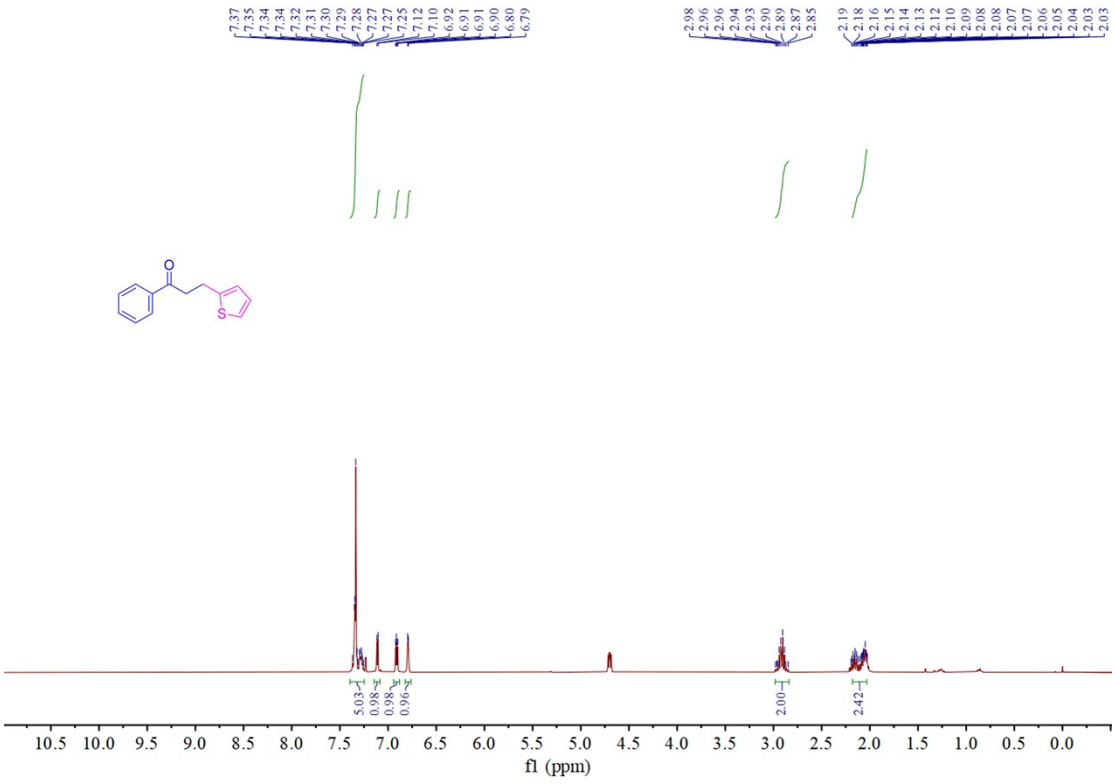

10. References

[1] G. Kresse and J. Furthmuller, *Phys. Rev. B*, 1996, **54**, 11169.

[2] J. P. Perdew, K. Burke and M. Ernzerhof, *Phys. Rev. Lett.*, 1996, **77**, 3865.

[3] B. Hammer, L. B. Hansen and J. K. Norskov, *Phys. Rev. B*, 1999, **59**, 7413.

[4] S. Grimme, *J. Comput. Chem.*, 2006, **27**, 1787-1799.